

~~Daily to annual~~ Application of a new net primary production ~~in~~ methodology; a daily to annual-scale data set for the North Sea ~~determined using~~, derived from autonomous underwater gliders and satellite Earth observation.

Benjamin R. Loveday^{1,2}, Timothy Smyth¹, Anil Akpınar³, Tom Hull^{4,6}, Mark E. Inall⁵, Jan Kaiser⁶, Bastien Y. Queste⁷, Matt Tobermann⁵, Charlotte A. J. Williams³, and Matthew R. Palmer³

¹Plymouth Marine Laboratory, Plymouth, UK

²Innoflair UG, Richard-Wagner-Weg 35, Darmstadt, Germany

³National Oceanography Centre, Liverpool, UK

⁴Centre for Environment, Fisheries and Aquaculture Science, Lowestoft, UK

⁵Scottish Association of Marine Science, Oban, UK

⁶Centre for Ocean and Atmospheric Sciences, School of Environmental Sciences, University of East Anglia, Norwich, UK

⁷Department of Marine Sciences, University of Gothenburg, Gothenburg, Sweden

Correspondence: Benjamin R. Loveday (ben.loveday@innoflair.com)

Abstract.

Shelf-seas play a key role in both the global carbon cycle and coastal marine ecosystems through the drawn-down and fixing of carbon, as measured through phytoplankton net primary production (NPP). Measuring NPP ~~in-situ~~ in situ, and extrapolating this to the local, regional and global scale presents challenges however because of limitations with the techniques utilised (e.g. radiocarbon isotopes), data sparsity and the inherent biogeochemical heterogeneity of coastal and open-shelf waters.

Here, we introduce a ~~powerful-new~~ new data set generated using a technique based on the synergistic use of ~~in-situ~~ in situ glider profiles and satellite Earth Observation measurements which can be implemented in a real-time or delayed mode system. We apply this system to a fleet of gliders successively deployed over a 19-month time-frame in the North Sea, generating an unprecedented fine scale time-series of NPP in the region (Loveday and Smyth, 2020). At the large-scale, this time-series gives close agreement with existing satellite-based estimates of NPP for the region and previous ~~in-situ~~ in situ estimates. What has not been elucidated before is the high-frequency, small-scale, depth-resolved variability associated with bloom phenology, mesoscale phenomena and mixed layer dynamics.

Copyright statement. This article is distributed under the Creative Commons Attribution 4.0 License

1 Introduction

15 Our understanding of the global ocean has been transformed over the past two decades by the advent of autonomous observations from gliders and floats (~~Chai et al., 2020; Roemmich et al., 2019; Mignot et al., 2014; Smith et al., 2011~~)(Chai et al., 2020; Roemmich et al., 2019; Mignot et al., 2014; Smith et al., 2011). Such platforms have shown the capability to probe the marine environment at increasingly fine temporal and spatial resolution at local, regional and global scales. Measuring Essential Ocean Variables (EOVs), such as temperature, salinity, chlorophyll-a fluorescence and photosynthetically available radiation (PAR), on these scales has greatly increased our ability to probe the

20 links between physical systems and primary productivity (Olita et al., 2017; Thomalla et al., 2015). Further, the adoption of autonomous platforms has improved the operational reach of traditional research vessels, which are typically cost and weather limited, and bound to a single point in space and time. ~~This is in contrast to~~ Alongside this, the international Argo float programme ~~which~~ has grown from zero to over 4,000 floats in a little over twenty years. This network now forms a critical part of the Global Ocean Observing System (GOOS) and assimilation of data from individual floats is crucial for global weather

25 forecast models (Le Traon et al., 2019). Currently, Argo floats are operationally constrained to the deep ocean (depth >2 km): gliders have no such constraint, although are around a factor of ten more expensive and require some form of piloting, rendering them less prevalent in the global ocean.

The past twenty years have also seen a revolution in space-based sensors, widely and generically termed as satellite Earth observation (SEO). Although SEO gives unprecedented global coverage, infra-red and optical sensors are limited to providing

30 data on the near surface (<1 μm to ~ 10 m; strictly, the first optical depth) and are therefore unable to resolve variability with depth of key features such as thermoclines and deep-chlorophyll maxima (Gordon and Clark, 1980; Morel and Berthon, 1989; Cullen, 2015). Additionally, passive optical and infra-red SEO coverage is limited by clouds blocking the surface view: ~~strategies~~. Strategies to overcome this shortcoming generally involve compositing multiple images of a region, which can lead to the smearing out of sharp ~~boundaries~~ eteboundaries separating physically and biogeochemically distinct water masses at

35 sub-kilometre to tens of kilometres scale resulting in an underestimate of spatial and temporal variability (Carr et al., 2006). The coastal domain also presents specific challenges for remote sensing of ocean colour in particular. Strong scattering, associated with high sediment loads, and absorption due to non-algal material and CDOM, make chlorophyll retrievals in Case-2 waters challenging (Morel et al., 2006; Sathyendranath et al., 2000). This complexity is compounded by the effects of bottom reflectance from shallow bathymetry (e.g. Ohde and Siegel, 2001) and chlorophyll signals that may be too high to be

40 interpreted by standard algorithms, resulting in excessive masking.

Where SEO missions excel is their ability to provide regional to global estimates of ocean state variables at rates on time-scales of days to decades, the latter depending upon the maturity of the measurement time-series. An example of this, and the subject of this manuscript, is net primary production (NPP), the carbon fixed by plants through photosynthesis: the basis of almost all terrestrial and marine food webs. NPP plays a critical role in Earth's climate system by regulating the draw-down

45 of atmospheric carbon dioxide (Parekh et al., 2006) and the air-sea exchange of radiatively important trace gases (Nightingale et al., 2000; Wanninkhof, 1992). SEO NPP algorithms widely estimate that marine phytoplankton fix carbon at a rate of 45–50 Gt a^{-1} (Carr et al., 2006) representing approximately half of all global NPP (Field et al., 1998). In contrast, ~~in-situ~~ in situ

measurements of NPP in the open ocean are sparse, are generally made in the more clement months of the year, and target interesting features such as upwelling zones (Joint et al., 2002) or seasonal phytoplankton blooms (Robinson et al., 2009).
50 Furthermore, regular fixed-point sampling (Barnes et al., 2015) is difficult to extrapolate due to spatial variability.

Significant improvements in NPP estimates from SEO surface chlorophyll-a concentration ([Chl-a]) fields are possible with simultaneous ~~in-situ~~ in situ chlorophyll fluorometry and PAR profiles (Jacox et al., 2015). Hemsley et al. (2015) demonstrated and validated in the North Atlantic, a method for estimating NPP at high vertical and temporal resolution, using glider chlorophyll fluorescence and irradiance profiles. Significantly, it used irradiance to calibrate fluorescence and, therefore, needed no
55 ~~in-situ~~ in situ samples for calibration. Hemsley et al. (2015) made possible depth-resolved continuous estimates of NPP over a full seasonal cycle, in all weathers.

In this paper we present a synergistic method, using a combination of ~~in-situ~~ in situ glider (Hemsley et al., 2015) and SEO, for estimating NPP at high vertical and temporal resolution. This method is translocatable to any region of the global ocean, and is designed to support processing in delayed (DM) and operational near real-time (NRT) modes. It allows for
60 flexible selection of algorithms to enable and, through the incorporation of SEO data, provides a consistent output despite inconsistent glider payloads or platform types. We apply this method to an 19-month autonomous glider field campaign in the North Sea, a critical shelf-sea for fisheries with other multiple environmental stressors including eutrophication (Ferreira et al., 2011), deoxygenation (Queste et al., 2016), shipping (Barry et al., 2006) and pollution (Salomons et al., 2012). ~~For the first time we~~ We uncover the considerable regional temporal and spatial variability in NPP, ~~driven by seasonal succession, fronts (Miller, 2009) and topographical features, as well as across this region,~~ capturing two winter seasons which are crucial in conditioning the system for the following spring and summer periods. We expect future analysis of this data set, the first of its kind for the region, to provide new insights into the biophysical interplay between NPP and a complex regional oceanography defined by the influences of strong tides, topography and fronts (Miller, 2009; Huthnance, 1991). The data set is made available via the British Oceanographic Data Centre (BODC), under <https://doi.org/10/fm39> (Loveday and Smyth, 2020).

70 2 Ingested glider data

As part of the Alternative Framework to Assess Marine Ecosystem Functioning in Shelf Seas (AlterEco) project, a sustained presence of autonomous underwater gliders in the North Sea was maintained between November 2017 and May 2019. The programme aimed to keep at least two gliders in the field at all times, to provide measurement redundancy and assist with data validation. All gliders had a basic instrumentation package consisting of Conductivity Temperature Depth (CTD) in order to
75 determine vertical profiles of temperature and salinity, and a Seabird Scientific ECO-puck for fluorescence and ~~back-scattering measurement~~ backscatter measurements. The data set presented here is confined to only those gliders with ECO-pucks configured for chlorophyll fluorescence ~~measurement~~ measurements. Beyond this, the payload of each individual glider differed depending on the requirements of the individual mission goals (figure 1a). Throughout the AlterEco campaign, the gliders occupied a consistent East-West (1.5° - 2.5°E, along 56.1°N) and North-South (55.2° - 56.2°N, along 2°E) transect (see figure
80 1b), with the southern extent of the latter venturing ~~on to~~ onto Dogger Bank.

AlterEco glider missions are grouped in seven deployments¹, outlined in table 1. The glider data for these deployments is available from the ~~British Oceanographic Data Centre (BODC)~~ at [BODC](https://www.bodc.ac.uk/data/bodc_database/gliders/) (https://www.bodc.ac.uk/data/bodc_database/gliders/). The data is supplied in the Everyone's Gliding Observatories (EGO) format², which aggregates all profiles from a single glider mission into one NetCDF file. [More information of the spatial coverage of each of the processed missions is given in table 2.](#)

3 Method

3.1 Overview of the NPP processor

The NPP processor comprises a set of Python-based routines that manage the ingestion, quality control, correction, and pre- and post-processing of autonomous underwater glider profiles, as well as interfaces with external routines to calculate spectral PAR (Gregg and Carder, 1990) and NPP itself (Morel, 1991), which are implemented in the C programming language. Figure 2 shows a detailed flow diagram for the various processing stages. The processor supports multiple approaches to NPP calculation, depending on the availability of glider-based optical sensor data. [Throughout this manuscript, when we refer to the NPP processor, we refer to the code routines that are represented in figure 2.](#)

At its heart, the algorithms used to calculate NPP are as described in Hemsley et al. (2015): these in turn draw heavily upon the spectral light NPP formulation of Morel (1991). However, this method is modified to cater for fluorescence quenching and light attenuation in shelf-seas, as opposed to the open ocean (as discussed in section 3.4). For the purposes of determining NPP, the optimal glider instrument payload consisted of (in order of importance) chlorophyll-a fluorescence, PAR and optical backscatter (Hemsley et al., 2015). Figure 1a shows that only four missions (497, 454, 499 and 517) had the full complement of required sensors, which necessitated modifications to the Hemsley et al. (2015) algorithms (see table 1).

3.2 Data acquisition and staging

The processing chain was designed to accommodate either near real-time mode (NRT) or delayed-time mode (DM) implementations, and as such ingests glider data either as individual NetCDF profiles as they become available (in NRT) or in EGO NetCDF format (in DM). The data set described here is processed in DM. Files may be ingested locally, or auto-downloaded from a remote FTP repository on a user determined schedule. All ingested source files are stored in an initial deployment directory, and catalogued in a centralised SQLite database. This non-destructive approach supports the continual updating of the glider record from a remote catalogue in the NRT case, while preventing replication. The database monitors, records and manages all subsequent stages of the processor.

NPP calculations are performed on a profile-by-profile basis. Glider data typically consists of both downward (dive) and upward (climb) components in a single file, which in our processing framework represents two profiles. If a pre-existing profile designation is provided, as is usually the case in EGO data, this is used to split the source data into profiles. If no designation

¹ [doi: available at https://doi.org/10.5285/b57d215e-065f-7f81-e053-6c86abc01a82](https://doi.org/10.5285/b57d215e-065f-7f81-e053-6c86abc01a82) and <https://doi.org/10.5285/86429662-97b8-74fa-e053-6c86abc0a97c>

² [fully described at http://doi.org/10.25607/OBP-768](http://doi.org/10.25607/OBP-768)

is provided, the ingested data is split into single files according to the turning points in the smoothed depth record. Smoothing is performed using a 5th order Savitzky–Golay filter, with a nominal window of ~~151 points~~ 51 points. This window, which represents 5-10 minutes in glider sampling time, does not relate to a particular physical scale, but is short enough to allow smoothing to accurately capture the transitions between descending and ascending dive components, but long enough to reduce incorrect dive splitting due to short inversions or “dwelling” at the top and bottom of dives. Individual profiles are then stored in the staging directory for future use.

3.3 Constructing Earth ~~Observation~~ observation trajectories

Due to trade offs necessary to achieve the multiple mission priorities of the AlterEco programme, not all gliders were able to accommodate PAR sensors. Here, when required, SEO-based PAR data is used in lieu of ~~in-situ measurements~~ in situ measurements (a substitution that is covered in more detail from section 3.3.1 onward). This increases both the flexibility and utility of the method for the operational oceanography community, allowing it to be applied to glider data where only ~~in situ~~ in situ chlorophyll-a fluorescence is available. In addition, SEO and reanalysis data is used to provide information on the prevailing atmospheric and marine conditions during each glider mission. A list of SEO and reanalysis data sources, and the variables that are extracted and/or derived can be found in table 3 and in figure 2.

When a glider mission is updated (e.g. a new profile is added in NRT mode), the processor calculates the new temporal and spatial extents of the mission. Using these extents, the processor gathers the required SEO and reanalysis data from the specified source, concatenates the retrieved catalogue in time and trims the spatial coverage to produce a 'data cube' that matches the glider mission extents. The spatial trimming is performed remotely, on the server side, if the data service in use allows this capability, reducing data transfer costs and time. In NRT mode, new data is added to extend the cube as required, without the need to download the entire catalogue once again (e.g. via the concatenation of new time slices to the existing local record). This operation is performed for all variables, for all gliders, irrespective of whether they have the relevant ~~in-situ~~ in situ measurement, allowing for the continual validation of the use of SEO and reanalysis data as a substitute.

Once the data cube has been constructed, the average time and location of each profile are extracted and concatenated into a one-dimensional time series of the glider trajectory. Bi-linear interpolation is then used to retrieve the corresponding SEO and reanalysis data from the relevant data cube, resulting in an SEO-trajectory file for each variable, with a value for each profile. During construction, the cube is both spatially and temporally 'padded' to eliminate 'edge effects' associated with interpolation.

3.3.1 Treatment of SEO PAR data trajectories

SEO-based broadband PAR values (E_d), defined as the average PAR value between 400 nm to 700 nm, are derived from MODIS daily average values, measured in $\text{mol m}^{-2} \text{d}^{-1}$ (Frouin et al., 1989) (see table 3). Instantaneous values of broadband PAR, corresponding to the glider measurement times, are derived from the average ~~values~~ daily value as follows. The light distribution is modelled as a sine curve between ~~dawn~~ sunrise ($T = 0$) and ~~dusk~~ sunset ($T = \pi$). The amplitude of this curve is determined such that the integrated value below it matches that of the daily average. The instantaneous value is then extracted

by interpolating the value from the curve at the glider measurement time, ~~and~~. The instantaneous PAR value is finally converted
145 to $W m^{-2}$.

3.4 Pre-processing and calibration

The pre-processing step consolidates the glider and SEO-based data on a profile-by-profile basis, performs quality control procedures and selects the relevant variables for NPP calculations depending on availability (figure 2). Sporadic missing values are common in in-situ-in situ data. Where possible, linear interpolation is used to fill these gaps in the positional, depth and
150 pressure data. If interpolation is not possible, the profile is discarded and no further processing takes place.

Following this, and where not provided directly, conservative temperature and absolute salinity are calculated from the glider CTD record using the TEOS-10 Python GSW toolbox ³. Mixed layer depth (MLD) is then calculated from the ~~density gradient~~
~~according to temperature and density gradients using a hybrid algorithm that accounts for profile shape, giving more accurate~~
~~estimates than threshold based methods that rely on a fixed value~~ Holte and Talley (2009). If the MLD calculation fails (eg.
155 due to missing depth data), the MLD from the previous profile is used. This is only allowed once. The MLD is prevented from being shallower than 5 m, as depths shallower than this are typically poorly sampled by a glider. Once the physical variables are processed, the PAR and [Chl-a] profiles are assessed, along with the ~~back-scattering~~ backscatter data, if present.

PAR data delivered in raw counts is corrected to $W m^{-2}$ using the calibration coefficients specific to the sensor. The in-situ
in situ [Chl-a] data ~~is similarly treated. In the latter case, calculated from sensor fluorescence, measure in units of volts, to units~~
160 of [Chl-a] by multiplying by the scale factor (calibration coefficient) specific to the sensor and subtracting the manufacturer
provided dark count. Backscatter is similarly calculated.

An additional dark correction is then applied to the [Chl-a] measurements. As all glider data in the AlterEco programme are
made available in delayed mode, the minimum value of [Chl-a] is extracted on a per-profile basis across the entire mission. To
remove the influence of large negative outliers, the global minimum value is then calculated as the three standard deviations
165 less than the mean value of the time series of profile minima. This value is then subtracted from the entire record. Throughout
the remaining processing, any [Chl-a] data is discarded where the calibrated value exceeds $1e^5 < 0.0$ $mg m^{-3}$. In the case of
DM processing, post-mission calibration factors can also optionally be applied, though none were applied are then assumed to
be erroneous and are discarded.

On rare occasions, glider 497 (Humpback) recorded occasional spikes of over $1e^3$ $mg m^{-3}$ in the [Chl-a] data. These
170 measurements are not considered to be reliable, and therefore all values over $1e^3$ $mg m^{-3}$ are discarded. In addition, glider 481
(Kelvin) experienced a sudden "step change" of > 5 $mg m^{-3}$ in [Chl-a] at depths below both the MLD and Z_{eu} as compared
with the initial deployment value, toward the end of its mission. Consequently, all data for this glider after this point are
discarded.

The NPP processor offers the possibility to introduce additional calibration factors, based on independent *in situ* measurements
175 taken at the time of glider deployment and recovery. Unfortunately, in the case of the AlterEco programme, no such measurements
were taken, and so no additional calibration of the [Chl-a] data is performed. To ensure that the manufacturer calibration is

³<https://teos-10.github.io/GSW-Python/>

sufficient in this case, the surface [Chl-a] data from each glider is compared with its SEO counterpart (3). The results are shown in figure 3. From the figure, it is evident that the, as expected, each glider shows significantly more variability than its SEO counterpart. However, for all gliders, the median value extracted from the glider is similar to its SEO counterpart. Further, with the exception of the Orca missions, the interquartile range for each glider overlaps with its SEO counterpart. This suggests that there is no significant bias in the glider [Chl-a] record, and that the manufacturer calibration was sufficient in most cases.

Where available, optical backscatter measurements (b_{bp}) may be used to correct the surface chlorophyll fluorescence profile for near-surface quenching (Hemsley et al., 2015). The backscatter data is initially passed through a 7-point running minimum filter to remove spikes (Thomalla et al., 2018). Negative values are removed and the backscatter profile is subsequently interpolated onto the glider depth record.

As with the treatment of the PAR and backscatter data, the [Chl-a] record is interpolated onto the glider depth record on a profile-by-profile basis. On occasion, due to very short dives, or quality control processes conducted on the original EGO format data, the [Chl-a] record is sparse to such an extent that interpolation onto the depth record is not possible. Where this occurs, the entire profile is discarded and no NPP calculation is performed.

3.4.1 Determining the PAR profile

PAR sensors do not always acquire at the same sampling rate as the glider CTD sensor. Consequently, where it is available *in situ-in situ* PAR data for a given profile is interpolated onto the glider depth record prior to further processing. The decision point for the use of glider or SEO-based broadband PAR is made as follows according to the prioritisation of the following 3 cases;

- Case 1: Where a profile falls during the day-time and glider E_d is available, this is used by default (though the use of SEO-PAR can be forced, to permit validation). K_{dPAR} is calculated from the linear regression of the logged PAR values with depth. The regression is weighted by the square-root of the magnitude of the logged PAR values, emphasising the effect of the surface layers. E_d at depth is then projected to the surface using the K_{dPAR} value, giving sub-surface near-surface broadband PAR (E_o^-).
- Case 1: Broadband PAR at the surface (or just above) (E_o^+) is then derived from E_o^- using ~~the method described in Hemsley et al. (2015)~~. ~~Fresnel reflectance is calculated using the wind speed, relative humidity and mean sea level pressure derived equation 2 from Hemsley et al. (2015) (equation 1, below).~~ A value of 0.04 is used for the irradiance reflectance, R (V. Hemsley, pers. comms.), and 0.48 for the Fresnel reflectance, \bar{r} . Total reflectance, r_{tot} , the sum of the direct reflectance (r_d) and diffuse reflectance (r_{diff}), is calculated via the method specified in the supplementary material of Hemsley et al. (2015). The required wind speed is provided from the SEO trajectory files.
- Case 2: Where glider PAR is not available, SEO-based surface broadband PAR (E_o^+) is substituted. E_o^- is ~~calculated as described in the previous step~~ then calculated as by rearranging equation 1. The same values as above are used for the irradiance reflectance and Fresnel reflectance. SEO $\overline{K_{dPAR}}$, calculated from SEO $\overline{K_{d490}}$ ~~Saulquin et al. (2013)~~, using

210 the turbid water exponential model described by equation 9a and 9b of (Saulquin et al., 2013). The calculated $\overline{K_{dPAR}}$ is then used to project broadband PAR into the subsurface across the glider depth record.

215 ~~Where Case 3: Although derived from the same source, SEO K_{d490} is occasionally not available, even though $\overline{K_{dPAR}}$ is calculated. In this case, the euphotic depth is determined according to equation 2 (Saulquin et al. (2013)), where (Lee et al., 2007), where CHL represents the maximum *in situ* [Chl-a] measured above the MLD. $\overline{K_{dPAR}}$ is then calculated according to 3, where $PAR(Z=Z_{eu})$ is assumed to be 1% of $PAR(Z=0)$, and the euphotic depth (Z_{eu}) is determined from the maximum *in situ* Chl-a above the MLD, according to equation 3 Lee et al. (2007).~~

$$\underline{E(0)^+} = \frac{\ln(PAR(0)) - \ln(PAR(Z_{eu}))}{Z_{eu}} \frac{E(0)^- (1 - R\bar{r})}{(1 - r_{tot})} \quad (1)$$

$$Z_{eu} = 34.0 \times CHL^{-0.39} \quad (2)$$

$$\underline{\overline{K_{dPAR}}} = \frac{\ln(PAR(Z=0)) - \ln(PAR(Z=Z_{eu}))}{Z_{eu}} \quad (3)$$

220 The PAR record is labelled as bad, and is not processed, in the case of i) night-time profiles, ii) ~~substantial gaps in the~~ where [Chl-a] data ~~could not be interpolated (see section 3.4)~~, or iii) where the glider is within 5 m of the bathymetry depth, as interpolated from the GEBCO 15 arc-second gridded product ⁴. The latter criteria prevents the glider from deriving NPP estimates from ~~Chl-a~~ readings that may have been gathered at depths where particle re-suspension ~~in is~~ likely to make ~~them~~ ~~unreliable.~~ ~~the PAR estimates derived from SEO unreliable, given that we assume a constant value of $\overline{K_{dPAR}}$.~~

225 ~~The calculation of Euphotic depth (Z_{eu}), a necessary parameter in some quenching algorithms, is dependent on the case being used. Under case 1, Z_{eu} is defined as the depth at which the light level is 1% of the surface light depth) is subsequently calculated value. Under case 2, Z_{eu} is calculated from $\overline{K_{dPAR}}$. Under case 3, Z_{eu} is calculated from equation 2. Z_{eu} is calculated for all good profiles, and is selectively used in the correction of the Chl-a profile. The case used is stored in the EUPHOTIC_DEPTH_FLAG variable of the final data set (please see table 4).~~

230 To validate this approach, ~~Figure ??~~ figure 4 a) and b) compares the ~~in situ~~ *in situ* (red) and SEO-based E_d E_a^+ (blue) estimates for gliders 517 (Cabot) and 454 (Cabot), respectively. ~~For both missions the SEO surface PAR around solar noon under-predicts the surface PAR reconstructed from the glider profiles by typically $\sim 50 \text{ W m}^{-2}$. In addition, the The SEO-based values do not take account of the instantaneous cloud conditions and, correspondingly, the standard deviation in the surface PAR time series is lower. However, the SEO-based interpolation method gives an accurate facsimile of the daily PAR cycle, with a mean \bar{E}_0^+ that falls within 7% of the in situ broadband value. This in situ value (an error value that is comparable with~~

⁴https://www.gebco.net/data_and_products/gridded_bathymetry_data/

235 the 5% "in air" performance of the *in-situ-in situ* PAR sensor itself⁵). However, it has a notably lower standard deviation. This is somewhat expected as the SEO-based values do not take account of the instantaneous cloud conditions.

3.4.2 Using the optical backscatter profile

Where available, optical backscattering measurements (b_{bp}) may be used to correct the surface chlorophyll fluorescence profile for near-surface quenching (Hemsley et al., 2015). The backscattering data is initially passed through a 7-point running minimum
240 ~~filter to remove spikes (Thomalla et al., 2018). Negative values are removed and the scattering profile is subsequently interpolated onto the glider depth record.~~ Across both missions, the SEO surface PAR under-predicts the surface PAR reconstructed from the glider profiles. At solar-noon, the nominal peak in the daily PAR value, this equates to an average anomaly of $\sim 50 \text{ W m}^{-2}$. However, the comparison of instantaneous values is problematic and overstates the discrepancy between the two time series. The daily integrated PAR time series align much more closely, with mean values from the glider (solid black line) / SEO
245 (dashed black line) of 5268 / 5041 kJ m^{-2} for 517 (Cabot) and 6265 / 6224 kJ m^{-2} for 454 (Cabot), respectively.

3.4.2 Quality control and quenching correction of the chlorophyll fluorescence profile

3.4.2 Quenching correction of the chlorophyll fluorescence profile

The glider chlorophyll data is initially screened for erroneous values, with measurements of $\text{Chl-a} < 0.0 \text{ mg m}^{-3}$ discarded. To account for bio-fouling, the record is also discarded where there is a consistent "step change" of $> 5 \text{ mg m}^{-3}$ in Chl-a at
250 depths below both the MLD and Z_{eu} , as compared with the initial deployment value. As with the treatment of the PAR data, the Chl-a is then interpolated onto the glider depth record on a profile-by-profile basis. Where the interpolation fails due to lack of data, the entire profile is discarded and no NPP calculation is performed.

Fluorescence quenching in phytoplankton is caused by a variety of physiological acclimation mechanisms in order to avoid photo-damage under excessive irradiance (Kiefer, 1973). This effect typically manifests as a depression of the fluorescence
255 signal in the surface waters during daylight, and particularly around solar noon when the downwelling irradiance is at a maximum (Xing et al., 2012; Biermann et al., 2015). Multiple approaches to quenching correction have been proposed, e.g. Xing et al. (2012); Biermann et al. (2015); Hemsley et al. (2015); Swart et al. (2015); Thomalla et al. (2018). The applicability of these methods depends on the region being studied and the availability of optical ~~backscattering~~ backscatter data. Four methods are tested for this data set;

- 260
- The Xing et al. (2012) method; where the maximum [Chl-a] measured in the mixed layer is projected to the surface for day-time profiles. This method can be used in either DM or NRT cases.
 - The Biermann et al. (2015) method; where the maximum [Chl-a] measured above the euphotic depth is projected to the surface for day-time profiles. This method can be used in either DM or NRT cases.

⁵<https://www.seabird.com/asset-get.download.jsa?id=54627862114>

- 265
- The Swart et al. (2015) method; where the optical [backscattering-backscatter](#) signal above the euphotic depth is used to correct the corresponding [Chl-a] on a profile by profile basis. This method can be used in either DM or NRT cases.
 - The Hemsley et al. (2015) method; where, again, the optical [backscattering-backscatter](#) signal is used to correct the corresponding [Chl-a] using the night-time relationship with [backscatteringbackscatter](#), as measured across the entire glider mission. This method can be used in DM cases, only.

270 Due to the lack of available light during night-time sampling, [Chl-a] profiles remain unquenched. The extensive variability in shelf-seas makes direct correction of day-time profiles to their nearest night-time counterpart challenging (Carberry et al., 2019). However, when quenching is appropriately accounted for day-time [Chl-a] profiles should, in the aggregate, approximate their night-time counterparts. Figure [??-5](#) compares the histogram distribution of night-time and day-time [Chl-a] profiles for [three-four](#) tested methods across the entire gliders 517 (Cabot) and 454 (Cabot) missions. Optical complexity in coastal waters, associated with the presence of sediment, undermines the relationships between [Chl-a] and the [backscattering-backscatter](#) record. Consequently, while it may perform well in the open ocean, the quenching correction method described by Hemsley et al. (2015) performs poorly in this case. The Swart et al. (2015) method ~~(not shown) is similarly unsuitable~~ [is shown to be similarly unsuitable for the same reason.](#)

275

The Xing et al. (2012) method clearly outperforms the other methods tested, and is used to process all the gliders deployed during the AlterEco programme. Its strong performance is ascribed to its ability to appropriately capture the regional seasonal interplay between the MLD and euphotic depth in the shelf seas. As shown in figure [??6](#), the MLD sits above the euphotic depth during spring. This allows for the establishment of a deep chlorophyll maxima (DCM) (see figure [??7](#)), which is particularly important for NPP in this region (Fernand et al., 2013). In this case, quenching corrections using euphotic depth as a maximum depth limit (e.g. (Biermann et al., 2015)) over-correct as they tend to encapsulate the DCM in the quenching correction process, extrapolating erroneously high [Chl-a] to the surface. [This is an understandable, as these approaches were indeed designed to account for sub-surface chlorophyll maxima, but in open ocean regions where the MLD is typically deeper than the \$Z_{eu}\$.](#)

285

3.5 Calculating and scaling the spectral irradiance profile

Once the pre-processing stages have been completed for all available glider profiles (figure 2) spectral E_d profiles are calculated for each [glider profile](#) using the solar irradiance model described by Gregg and Carder (1990). To account for local meteorological conditions, the model runs using the [total column atmospheric ozone](#) ($[O_3]$), cloud cover, wind speed, relative humidity and total column water vapour parameters for each profile, stored in the relevant trajectory file ([Table-table](#) 3). These spectral E_d values calculated from the model are scaled such that their integrated value between 400 nm and 700 nm matches the corresponding E_o^+ measurements provided by the glider or SEO data sources (see section 3.4.1). This scaling correction accounts for instantaneous sky conditions associated with each profile.

290

3.6 Implementing chlorophyll-a scaling

295 The work by Hemsley et al. (2015) implemented a novel methodology to exploit the relationship between PAR and [Chl-a] to account for changes in the apparent fluorescence to chlorophyll calibration, brought about by phytoplankton community succession. This approach allows dynamic changes to the calibration, and reduces the need for in-field calibration, which is difficult, if not impossible to implement, especially in the near real-time case. However, this method is based on an in water model suitable for Case-1 waters (Carr, 1986), with the non-water component of light attenuation ascribed to [Chl-a] only
300 (Morel and Maritorena, 2001).

The processor retains the ability to implement this method, as detailed extensively in Hemsley et al. (2015) and represented in [Figure figure 2](#) by the "Case 1" decision box. However, the optically complex waters of the shelf-seas are rich in sediment, and do not conform to the Case-1 paradigm. Implementation of a spectral irradiance model more suitable to the region requires the consistent deployment of ~~in situ PAR and back-scattering~~ [in situ PAR and backscatter](#) sensors that is not available across
305 the AlterEco programme. Consequently, no PAR-based scaling of the [Chl-a] profiles is performed for this data set. This caveat is further discussed in section 5.4.

3.7 Calculating NPP

Net primary production is calculated from the corrected [Chl-a] and ~~depth profiles and~~ spectral downwelling PAR ~~for each profile~~ [profiles](#) using the Morel (1991) model, as presented in Hemsley et al. (2015) and shown in equation 4. The model
310 calculates NPP through a triple integral across day length (L), depth ($D_1 = 0$, $D_2 = Z_{eu}$) and wavelength ($\lambda_1 = 400$ nm, $\lambda_2 = 700$ nm). The absorption cross section per unit of chlorophyll (a^* [m^{-1}]) and net growth rate (ϕ_μ [$\text{mol}(\text{carbon}) \text{mol}(\text{quanta})^{-1}$]) are parameterised as in (Morel, 1991).

$$NPP = 12 \int_0^L \int_{D_1}^{D_2} \int_{\lambda_1}^{\lambda_2} [\text{Chl-a}](Z) E_d(t, Z, \lambda) a^*(\lambda) \phi_\mu(t, Z, \lambda) d\lambda dZ dt \quad (4)$$

NPP estimates, in units of carbon flux ($\text{mg m}^{-3} \text{d}^{-1}$), are calculated for all ~~uncorrected and~~ corrected [Chl-a] profiles, using
315 the per-profile average time and position for each. The piece-wise measurements are integrated from the 1% light level (as determined by the model) to the surface to give a final estimate of depth integrated primary productivity in carbon flux of $\text{mg m}^{-2} \text{d}^{-1}$.

[Figure ?? 8](#) allows a comparison of using SEO-based PAR in the calculation of spectral E_d and, ~~subsequently~~ [subsequent](#) NPP, in contrast to using ~~in situ~~ [in situ](#) PAR. SEO-based PAR is shown to function as a suitable proxy in this method, remaining
320 highly correlated with its ~~in situ~~ [in situ](#) counterpart, with mean values that are within 2% of the target estimate.

When combined, the NPP times series derived from the AlterEco glider deployments spans a 19-month period, as shown in [figure ??](#). ~~Two peaks are captured in April/May 2018 and April 9. As expected, NPP is at its greatest in the spring and early summer, reaches its highest in the spring of 2019, corresponding with the timing of the regional spring bloom, and with the latter event significantly more intense. Independent Chl-a estimates, derived from v4.2 of the ESA Ocean Colour Climate~~

325 ~~Change Initiative (OC-CCI) data set (Sathyendranath et al., 2019), indicate that the 2018 spring bloom was relatively intense, suggesting that 494 (Stella) failed to fully capture this event. As expected, NPP drops to . Conversely, it drops to~~ near zero in the winter months, when light availability becomes limiting. The figure also shows the inherent spatial and temporal variability in the time series, reflected in the inter-glider and intra-glider data, respectively. Despite operating during the same period, glider 454 (Cabot) measures approximately twice the NPP of glider 455 (Orca) throughout April, May and June of 2018, where we expect biological activity to be near its highest level.

330 Black traces, indicating NPP estimates derived from ~~in situ~~ in situ PAR sensors, compare well with their coloured (SEO derived) counterparts in all cases. However, the divergence between the signals recorded by the concurrently deployed gliders 455 (Orca), 497 (Humpback) and 454 (Cabot) strongly suggests the presence of significant ~~spatial heterogeneity variability~~ in the region north of the Dogger Bank (1, South East corner).

335 4 Data provenance and structure

The complete finalised data set consists of 13 netCDF files, in EGO format. Each netCDF file corresponds to a single glider mission. The data covers a region spanning a longitude of -1.497° W to 2.577° E, a latitude of 51.005° N to 58.669° N and a time period of 15/11/2017 to 28/05/2019. During deployment 481 (Kelvin) the glider remained at the surface from 21/11/2018 to 02/12/2018 and did not acquire [Chl-a] data and so no NPP was calculated for this period. No other glider was deployed during this time, resulting in a single ~~10-day~~, 10-day gap in the record. Each EGO data file, contains the variables listed in table 4. The intermediate variables calculated as part of the processor as not included in the netCDF data files. However, intend to publish the NPP processor in full, allowing future users to make use of it and adapt the methodology to their own purposes. More information on the availability of the code can be found in the Code and Data availability section of this manuscript. It is important to note that, to avoid duplication, each netCDF output file does not include the temperature and salinity variables used in the NPP processor. However, these can be found via BODC at the following link [https://www.bodc.ac.uk/data/bodc_](https://www.bodc.ac.uk/data/bodc_database/gliders/)
340 database/gliders/, and have a one-to-one mapping to the NPP glider dataset. The specific links for each glider are included in the final column of table 1.

345 Responsibility for maintaining the data set lies with Plymouth Marine Laboratory, the provenance authority for the final output. No updates of the data set are expected. The data set is stored in the British Oceanographic Data Centre (BODC) archive, and has the following digital object identifier: <https://doi.org/10.5285/b58e83f0-d8f3-4a83-e053-6c86abc0bbb5>.

5 Data validity

5.1 Fluorescence quenching validity

In order to quantify the efficacy of the various quenching correction algorithms upon the chlorophyll fluorescence profiles, a comparison was made between the day-time (quenched) and night-time (not quenched) [Chl-a] over the top 20m of the water column. This comparison assumes that there is little change in the vertical profile of [Chl-a] in a 24 hour period: this is
355

obviously a simplification as there will be changes due to (1) bloom growth or [decay and loss \(e.g. via respiration, decay and grazing\)](#) and (2) spatial variability. Figure [??-5](#) shows that the major discrepancy between the night-time and the uncorrected day-time [Chl-a] profiles, for glider 454 (Cabot: see [Figure 1 and Table figure 1 and table 1](#)), is when the integrated [Chl-a] in the top 20 m exceeds [5.4](#) mg m⁻² and is less than ~ 12 mg m⁻². The percentage variance between day-time and night-time [eases](#) uncorrected cases is 91.0% with a significance p value of <0.01. The Xing et al. (2012) method ([Figure ??figure 5](#)) clearly outperforms the other correction methods tested in this case ($r^2 = 97.8\%$ $p < 0.01$; cf. Hemsley et al. (2015) $r^2 = 32.8\%$ $p < 0.01$ and; Biermann et al. (2015) $r^2 = 0.2\%$ $p = 0.81$). Similar results were obtained for glider 517 (Cabot: see [Figure 1 and Table figure 1 and table 1](#)) with for uncorrected ($r^2 = 92.7\%$ $p < 0.01$) and Xing et al. (2012) ($r^2 = 97.8\%$ $p < 0.01$); the other two algorithms interchanged their ranking however with Biermann et al. (2015) ($r^2 = 73.3\%$ $p < 0.01$) and Hemsley et al. (2015) ($r^2 = 26.2\%$ $p < 0.01$).

Figure [??-7](#) shows the corrected [Chl-a] profiles for glider 454 (Cabot). The corrected time-series shows a gradual deepening of the DCM over the three month mission from around 25 m in mid-May (2018) to 40 m in mid-August. During this period there is also a clear reduction in the peak [Chl-a]: >3 mg m⁻³ at the start of the mission, ~1 mg m⁻³ towards the end. The transects on and off Dogger Bank (depths shoaling to around 40 m) are clearly correlated with a shoaling of the euphotic depths from ~ 30 m on the Bank to ~ 50 m off the Bank. Changes in the MLD are less pronounced, apart from a deepening between June 18 and 22 2018, and a rapid shoaling from 30 to 18 m around 24 June 2018. Meteorologically, June 2018 was characterised by relatively slack pressure gradient (light winds) until a brief three day period of stronger north or north-westerly winds on 19/22 June which corresponds to the episodic deepening of the MLD in this period.

5.2 Comparison with historical measurements in the North Sea

Two distinct advantages of gliders are that they sample flexibly, in terms of horizontal space and depth, and they can gather data at high frequency. As there are no pre-existing measurements of NPP in the North Sea with comparable frequency, here we compare our results with available estimates of annual mean productivity [-from both satellite and in situ sources.](#)

[Independent \[Chl-a\] estimates, derived from v4.2 of the ESA Ocean Colour Climate Change Initiative \(OC-CCI\) data set \(Sathyendranath et al., 2019\), indicate that the 2018 spring bloom was relatively intense in comparison to 2019; a fact that does not appear to be reflected in the glider NPP data. Kulk et al. \(2020\) applied the NPP methodology of Platt and Sathyendranath \(1988\) and Sathyendranath et al. \(2020\) to this satellite \[Chl-a\] record, producing a 20 year time series of satellite-based NPP from 1998-2018. Although this record does not span the entire AlterEco period \(2017-2019\), is only calculated at 9 km resolution, and is only available as a monthly product, it provides a useful data source to compare the glider NPP measurements against. Satellite-based NPP estimates for each glider are shown in the light orange on Figure 9. Comparing the glider and co-located satellite time-series further suggests that 494 \(Stella\) likely failed to fully capture the onset of the spring bloom in 2018. However, given the disparity between the estimates obtained by 454 \(Cabot\), 494 \(Stella\) and 497 \(Humpback\), it is likely that the region is subject to significant spatial heterogeneity, which perhaps the satellite product is too coarse to record.](#)

Table 5 summarises the monthly and annual NPP estimates across all [AlterEco glider](#) campaigns. The [monthly mean and standard deviations derived from the satellite NPP record, calculated across a box spanning the AlterEco sampling region, are](#)

390 shown in the final two columns of table. The annual cycle and mean annual NPP rate as measured from the glider missions
agrees well with contemporaneous values interpolated from the monthly mean OC-CCI ~~based NPP climatology for 1998-2018~~
~~(Kulk et al., 2020)NPP record~~. It is notable from the table that, while still within one standard deviation, the April NPP peak
in the glider data is somewhat lower than its OC-CCI counterpart, likely ~~as a result of~~ due to the low signal recorded by 494
(Stella) over this period in 2019. ~~The~~ However, the glider-based NPP signal peaks at a time consistent with remote sensing
395 estimates.

The glider-based annual mean NPP value $98 \text{ gC m}^{-2}\text{a}^{-1}$ ~~is comparable~~. This compares favourably with the $119 \text{ gC m}^{-2}\text{a}^{-1}$
measured by Joint and Pomroy (1993), who applied a C^{14} approach to measure daily NPP through extensive surveys carried
out over ICES Region 7 (north of Dogger Bank) ~~by Joint and Pomroy (1993), as well as with observation based estimates of,~~
scaling up to monthly estimates using the mean daily value across the region and number of days per month. It also compares
400 well to the annual estimate of $125 \text{ gC m}^{-2}\text{a}^{-1}$ for the northern North Sea (~~van Beusekom and Diel-Christiansen, 1994~~) proposed
by van Beusekom and Diel-Christiansen (1994), based on a synthesis of daily NPP estimate from multiple cruises. The glider
measurements are similarly consistent with NPP estimates derived from models; with Varela et al. (1995) recording 130 gC
 $\text{m}^{-2}\text{a}^{-1}$ for ICES Region 7 (as used by ~~Joint and Pomroy (1993)~~ Joint and Pomroy, 1993), Moll (1998) simulating 119 gC
 $\text{m}^{-2}\text{a}^{-1}$ across the northern North Sea and Zhao et al. (2019) reporting $82.6 - 118.8 \text{ gC m}^{-2}\text{a}^{-1}$ for the central and northern
405 North Sea in their tidal simulations.

Alongside NPP, Varela et al. (1995) provides estimates of gross primary production (GPP). In the northern North Sea (ICES
region 4), an NPP of $149 \text{ gC m}^{-2}\text{a}^{-1}$ is associated with a GPP of $314 \text{ gC m}^{-2}\text{a}^{-1}$. ~~Similar modification of the glider based~~
Assuming that the ratio of NPP:GPP remains broadly constant in the region on an annual basis, we can apply this to our
glider NPP measurements to obtain a GPP estimates ~~suggests of~~ an approximate value of $\sim 200 \text{ gC m}^{-2}\text{a}^{-1}$. This compares
410 favourably with the measurements of Capuzzo et al. (2018), who reported an annual mean gross production of $200 \pm 15 \text{ gC}$
 $\text{m}^{-2}\text{a}^{-1}$ in seasonally stratified regions from 1998 to 2013 (including Dogger Bank).

5.3 Value and utility

Primary production is highly variable on short temporal and spatial scales. The impact of the mesoscale variability associated
with fronts (Olita et al., 2017; Taylor and Ferrari, 2011) and eddies (Hansen et al., 2010; Hu et al., 2014) can be extensive. High
415 frequency changes in tidal phase (Zhao et al., 2019), sky conditions and the local wave field (Reed et al., 2011) can also exert a
strong influence. To monitor the impact of these processes in highly productive shelf seas, it is desirable to continually sample
key regions using technologies that support adaptive sampling strategies. Autonomous underwater vehicles (AUVs), such as
gliders, offer one such approach to this problem, offering persistent monitoring of shelf sea biogeochemistry (Chai et al., 2020;
Liblik et al., 2016) and informing regional model assimilation strategies (Skákala et al., 2021).

420 This data set presents the first intra-annual, glider-based ~~in situ~~ in situ NPP time series for the North Sea, that is able to address
questions pertaining to biophysical interactions on a high-frequency basis. From figure ~~??~~ 9 it is clear that the NPP signal is
modulated at multiple frequencies within individual deployments, and substantial spatial heterogeneity exists between co-

deployments (e.g. 455 (Orca) and 454 (Cabot)). Further analysis of this data set should give insight into the physical processes that contribute to this variability.

425 When deployed with multiple mission goals in mind, glider payload space typically comes at a premium. Most notable in this case, is the effect on the deployment of PAR sensors, which are present on less than 50% of missions. However, adaptation of previous methodology to accommodate SEO based PAR estimates has been shown to be feasible. Combining SEO surface data with AUV profiles also presents interesting options for reconstructing subsurface fields. Machine learning methods have demonstrated the feasibility of combining SEO surface fields with ~~in-situ-profile~~ [in situ profiles](#) to render a three dimensional
430 picture of ocean biogeochemical properties (Sauzède et al., 2015, 2016). The data set presented here would be well suited for application of such methods to evaluate and further extend coverage of NPP data in the global ocean.

The processing method developed here allows for glider-based NPP to be calculated in a much broader array of cases. While in DM it can replicate the approach of Hemsley et al. (2015), the inclusion of differing quenching algorithms promotes applica-
tion to different regions and/or different sensor loads (e.g. those without ~~back-scattering~~ [backscatter](#)). The flexible inclusion of
435 SEO data in lieu of ~~in-situ~~ [in situ](#) PAR measurements expands this utility even further, allowing NPP calculations from gliders with a more limited array of sensors without substantial loss of accuracy (~~Figure ??~~ [figure 8](#)). Finally, the ability to support NRT ingestion of glider data allows for NPP calculation in an operational setting.

5.4 Limitations, scope and future improvements

PAR, when spectrally decomposed, can be used to provide a calibration of the [Chl-a] fluorometer (Hemsley et al., 2015).
440 Although the fluorometer calibration may be accurate at the start of an individual mission, calibration using nearby discrete [Chl-a] samples at launch and retrieval of the glider may lead to a false sense of security, particularly in areas of high heterogeneity, such as experienced during this study. Hemsley et al. (2015) showed that within mission variability in the correction factor is possible due to changes in phytoplankton community structure. However, the model previously proposed is suitable for case-1 waters only, and does not account for absorption and scattering by CDOM and sediment, respectively, and so no
445 dynamic calibration is applied here. The strong agreement between AlterEco glider NPP measurements and both satellite and historical ~~in-situ~~ [in situ](#) estimates (see section 5.2) underlines the validity of the data set, and future work will consider the incorporation of a model to cater for more complex waters, where glider payload allows.

As noted in the 3.4 section, the measurement of in situ dark counts for fluorescence is performed on the entire glider mission. This method is, therefore inappropriate for near-real analysis of glider profiles. Inclusion of a methodology to
450 calculate dark counts for both the fluorescence and backscatter measurements on a per-profile basis, such as that developed by Wojtasiewicz et al. (2018), would also be advantageous.

While the quenching correction method of Xing et al. (2012) proved most appropriate in this case, this result should not be a considered a general solution. This rationale underpins the decision to incorporate multiple methods to correct near surface fluorescence, however, the eventual method chosen is limited by the sensors deployed, most notably the availability of
455 ~~backscattering data~~ (~~Figure~~ [backscatter data \(figure 1\)](#)). The availability of ~~back-scattering~~ [backscatter](#) data allows for the a wider selection of correction methodologies in both DM (~~Thomalla et al., 2018; Hemsley et al., 2015~~) and NRT (~~Swart et al., 2015~~).

~~processing~~ processing (Hemsley et al., 2015) and NRT processing (Swart et al., 2015). In addition, its inclusion is essential to constructing a complex water model, as discussed earlier in this section. As the NPP processor was developed during the AlterEco programme, which commenced in 2017, it only takes advantage of quenching methods available at the time. Future work is expected to include more recent quenching methodologies such as (Thomalla et al., 2018).

460 For long duration missions (i.e. more than a few days) bio-fouling of sensors mounted on gliders can affect data quality. Unlike Argo floats, which typically park at depths well below the euphotic zone (~1 km), for 10 days, gliders spend a greater portion of their time in the photic zone, allowing the build-up of a bacterial substrate and then algal colonisation. Despite many strategies to mitigate bio-fouling (copper covered sensors, bio-wipers), it is impossible to completely eradicate it currently, and
465 even predicting its onset is problematic. Anecdotally on moorings situated in the western English Channel (Smyth et al., 2010a, b), bio-fouling has been observed to take several months to colonise sensors, and then following cleaning, has only taken a few weeks to re-emerge. Best efforts have been made to truncate the glider [Chl-a] record where bio-fouling appears evident (section 3.4.2).

Here, the methodology described is used to generate a primary productivity data set in an optically complex shelf-region.
470 However, much of the basis of the methodology is derived from previous work that was developed for use in the open ocean context (e.g. Hemsley et al. (2015)). Consequently, we expect that the NPP processor to be viable in the open ocean, where chlorophyll concentration tends to dominate the optical signal. In the open ocean, quenching methods based on calibration against the backscatter record are also likely to perform better (e.g. Swart et al. (2015)), and, in the case of Hemsley et al. (2015), allow for dynamic calibration associated with changes in phytoplankton community structure. As Earth observation-based
475 retrieval of chlorophyll concentration typically has lower errors in the open ocean, there may be opportunities to investigate the use of remotely sensed data to correct, and dynamically calibrate the *in situ* chlorophyll record, an approach previously suggested by Lavigne et al. (2012). It is, however, important to point out that the methodology may require tuning when used in different mission contexts. With deeper and/or longer dives, care should be given to select the correct smoothing parameters to determine the turning points of the profile. In addition, where *in situ* PAR is not available, it may also be advisable to select
480 a $\overline{K_{dPAR}}$ model that is more suited to clear waters, such as Morel et al. (2007). More broadly, future investigations should also consider the effect that the choice of $\overline{K_{dPAR}}$ model used has on the resulting NPP value.

6 Conclusions

This paper discusses the generation of ~~an~~-a 19-month, near-continuous glider-based data set of net primary production in the North Sea; the first of its kind for the region. The methodology used to derive this time-series is discussed in detail, with
485 specific focus on the approaches taken to account for fluorescence quenching and the use of SEO-based PAR data in lieu of ~~in-situ~~*in situ* sensors. While, in this case, pre-processed glider data from the AlterEco programme serves as a starting point, consideration is also given to adaptation of the method for NRT and operational use. Although limitations in the approach used are discussed, especially in regard to the feasibility of dynamic calibration and effects of biofouling, the results show strong agreement with previous studies as well satellite derived estimates and the results of biogeochemical model simulations. They

490 present a unique, depth-resolved picture of the high-frequency variability and spatial heterogeneity present in the **production**
in rates of NPP for the region and highlight the advantages of using autonomous systems to persistently monitor the shelf-seas,
especially in tandem with remote sensing based approaches. The newly developed processing approach also has implications
for the development of a PP indicator (e.g. through the Marine Strategic Framework Directive food web descriptor), overcoming
some of the temporal and spatial sampling limitations that have historically undermined its inclusion in assessments, relegating
495 its listing to candidate only.

7 Code and data availability

The data is made available via the British Oceanographic Data Centre (BODC), via <https://doi.org/10/fm39>. Its use may be cited using Loveday and Smyth (2020). Access to the code for the primary productivity processor will shortly be made available via <https://github.com/timjsmyth/GliderPP>.

500 *Author contributions.* Ben Loveday and Tim Smyth developed the methodological approach and led writing of the manuscript. Ben Loveday built the processing system and generated the resulting data set. The remaining authors are responsible for the glider deployments, the provision of supporting data sets and calibration information, and for providing methodological input in the manuscript.

Competing interests. The authors declare that they have no competing interests.

Acknowledgements. This work was funded by the NERC Alternative Framework to Assess Marine Ecosystem Functioning in Shelf Seas
505 (AlterEco) programme under grant numbers NE/P013899/1, NE/P013910/1 and NE/P013902/1. The authors thank Emma Slater for managing data ingestion and hosting at BODC; Dr. Thomas Jackson at Plymouth Marine Laboratory for providing the OC-CCI data used in table 4, and Dr 5 and figure 9, Dr. Hayley Evers-King for proof reading and comments on the manuscript narrative. We are also grateful to our two anonymous reviewers, and especially Dr. Sandy Thomalla, for their insightful comments and suggestions for improvements.

References

- 510 Barnes, M. K., Tilstone, G. H., Suggett, D. J., Widdicombe, C. E., Bruun, J., Martinez-Vicente, V., and Smyth, T. J.: Temporal variability in total, micro-and nano-phytoplankton primary production at a coastal site in the western English Channel, *Progress in Oceanography*, 137, 470–483, 2015.
- Barry, M., Elema, I., and Van Der Molen, P.: Governing the North Sea in the Netherlands, *Administering Marine Spaces: International Issues*, p. 64, 2006.
- 515 Biermann, L., Guinet, C., Bester, M., Brierley, A., and Boehme, L.: An alternative method for correcting fluorescence quenching, *Ocean Science*, 11, 83–91, 2015.
- Capuzzo, E., Lynam, C. P., Barry, J., Stephens, D., Forster, R. M., Greenwood, N., McQuatters-Gollop, A., Silva, T., van Leeuwen, S. M., and Engelhard, G. H.: A decline in primary production in the North Sea over 25 years, associated with reductions in zooplankton abundance and fish stock recruitment, *Global Change Biology*, 24, e352–e364, 2018.
- 520 Carberry, L., Roesler, C., and Drapeau, S.: Correcting in situ chlorophyll fluorescence time-series observations for nonphotochemical quenching and tidal variability reveals nonconservative phytoplankton variability in coastal waters, *Limnology and Oceanography: Methods*, 17, 462–473, 2019.
- Carr, M.-E., Friedrichs, M. A., Schmeltz, M., Aita, M. N., Antoine, D., Arrigo, K. R., Asanuma, I., Aumont, O., Barber, R., Behrenfeld, M., et al.: A comparison of global estimates of marine primary production from ocean color, *Deep Sea Research Part II: Topical Studies in Oceanography*, 53, 741–770, 2006.
- 525 Carr, M. R.: Modelling the attenuation of broad band light down a water column, *Journal of the Royal Statistical Society: Series D (The Statistician)*, 35, 325–333, 1986.
- Chai, F., Johnson, K. S., Claustre, H., Xing, X., Wang, Y., Boss, E., Riser, S., Fennel, K., Schofield, O., and Sutton, A.: Monitoring ocean biogeochemistry with autonomous platforms, *Nature Reviews Earth & Environment*, 1, 315–326, 2020.
- 530 Cullen, J. J.: Subsurface chlorophyll maximum layers: enduring enigma or mystery solved?, *Annual Reviews*, 2015.
- Fernand, L., Weston, K., Morris, T., Greenwood, N., Brown, J., and Jickells, T.: The contribution of the deep chlorophyll maximum to primary production in a seasonally stratified shelf sea, the North Sea, *Biogeochemistry*, 113, 153–166, 2013.
- Ferreira, J. G., Andersen, J. H., Borja, A., Bricker, S. B., Camp, J., Da Silva, M. C., Garcés, E., Heiskanen, A.-S., Humborg, C., Ignatiades, L., et al.: Overview of eutrophication indicators to assess environmental status within the European Marine Strategy Framework Directive, *Estuarine Coastal and Shelf Science*, 93, 117–131, 2011.
- 535 Field, C. B., Behrenfeld, M. J., Randerson, J. T., and Falkowski, P.: Primary production of the biosphere: integrating terrestrial and oceanic components, *Science*, 281, 237–240, 1998.
- Frouin, R., Lingner, D. W., Gautier, C., Baker, K. S., and Smith, R. C.: A simple analytical formula to compute clear sky total and photosynthetically available solar irradiance at the ocean surface, *Journal of Geophysical Research: Oceans*, 94, 9731–9742, 1989.
- 540 Gordon, H. R. and Clark, D. K.: Remote sensing optical properties of a stratified ocean: an improved interpretation, *Applied Optics*, 19, 3428–3430, 1980.
- Gregg, W. W. and Carder, K. L.: A simple spectral solar irradiance model for cloudless maritime atmospheres, *Limnology and Oceanography*, 35, 1657–1675, 1990.
- Hansen, C., Kvaleberg, E., and Samuelsen, A.: Anticyclonic eddies in the Norwegian Sea; their generation, evolution and impact on primary production, *Deep Sea Research Part I: Oceanographic Research Papers*, 57, 1079–1091, 2010.
- 545

- Hemsley, V. S., Smyth, T. J., Martin, A. P., Frajka-Williams, E., Thompson, A. F., Damerell, G., and Painter, S. C.: Estimating oceanic primary production using vertical irradiance and chlorophyll profiles from ocean gliders in the North Atlantic, *Environmental Science & Technology*, 49, 11 612–11 621, 2015.
- 550 Holte, J. and Talley, L.: A new algorithm for finding mixed layer depths with applications to Argo data and Subantarctic Mode Water formation, *Journal of Atmospheric and Oceanic Technology*, 26, 1920–1939, 2009.
- Hu, Z., Tan, Y., Song, X., Zhou, L., Lian, X., Huang, L., and He, Y.: Influence of mesoscale eddies on primary production in the South China Sea during spring inter-monsoon period, *Acta Oceanologica Sinica*, 33, 118–128, 2014.
- Huthnance, J.: Physical oceanography of the North Sea, *Ocean and shoreline management*, 16, 199–231, 1991.
- Jacox, M. G., Edwards, C. A., Kahru, M., Rudnick, D. L., and Kudela, R. M.: The potential for improving remote primary productivity estimates through subsurface chlorophyll and irradiance measurement, *Deep Sea Research Part II: Topical Studies in Oceanography*, 112, 107–116, 2015.
- 555 Joint, I. and Pomroy, A.: Phytoplankton biomass and production in the southern North Sea, *Marine Ecology-Progress Series*, 99, 169–169, 1993.
- Joint, I., Groom, S. B., Wollast, R., Chou, L., Tilstone, G. H., Figueiras, F. G., Loijens, M., and Smyth, T. J.: The response of phytoplankton production to periodic upwelling and relaxation events at the Iberian shelf break: estimates by the ^{14}C method and by satellite remote sensing, *Journal of Marine Systems*, 32, 219–238, 2002.
- 560 Kiefer, D.: Chlorophyll a fluorescence in marine centric diatoms: responses of chloroplasts to light and nutrient stress, *Marine Biology*, 23, 39–46, 1973.
- Kulk, G., Platt, T., Dingle, J., Jackson, T., Jönsson, B. F., Bouman, H. A., Babin, M., Brewin, R. J., Doblin, M., Estrada, M., et al.: Primary production, an index of climate change in the ocean: satellite-based estimates over two decades, *Remote Sensing*, 12, 826, 2020.
- 565 Lavigne, H., D’ortenzio, F., Claustre, H., and Poteau, A.: Towards a merged satellite and in situ fluorescence ocean chlorophyll product, *Biogeosciences*, 9, 2111–2125, 2012.
- Le Traon, P. Y., Reppucci, A., Alvarez Fanjul, E., Aouf, L., Behrens, A., Belmonte, M., Bentamy, A., Bertino, L., Brando, V. E., Kreiner, M. B., et al.: From observation to information and users: the Copernicus Marine Service perspective, *Frontiers in Marine Science*, 6, 234, 2019.
- 570 Lee, Z., Weidemann, A., Kindle, J., Arnone, R., Carder, K. L., and Davis, C.: Euphotic zone depth: Its derivation and implication to ocean-color remote sensing, *Journal of Geophysical Research: Oceans*, 112, 2007.
- Liblik, T., Karstensen, J., Testor, P., Alenius, P., Hayes, D., Ruiz, S., Heywood, K., Pouliquen, S., Mortier, L., and Mauri, E.: Potential for an underwater glider component as part of the Global Ocean Observing System, *Methods in Oceanography*, 17, 50–82, 2016.
- 575 Loveday, B. R. and Smyth, T.: An Alternative Framework to Assess Marine Ecosystem Functioning in Shelf Seas (AlterEco) Primary productivity estimates derived from ocean glider in situ sensors and photosynthetically available radiation estimates from in situ and satellite data between November 2017 and May 2019 in the North Sea, British Oceanographic Data Centre, National Oceanography Centre, NERC, UK, https://www.bodc.ac.uk/data/published_data_library/catalogue/10.5285/b58e83f0-d8f3-4a83-e053-6c86abc0bb5/, 2020.
- 580 Mignot, A., Claustre, H., Uitz, J., Poteau, A., d’Ortenzio, F., and Xing, X.: Understanding the seasonal dynamics of phytoplankton biomass and the deep chlorophyll maximum in oligotrophic environments: A Bio-Argo float investigation, *Global Biogeochemical Cycles*, 28, 856–876, 2014.

- Miller, P.: Composite front maps for improved visibility of dynamic sea-surface features on cloudy SeaWiFS and AVHRR data, *Journal of Marine Systems*, 78, 327–336, 2009.
- 585 Moll, A.: Regional distribution of primary production in the North Sea simulated by a three-dimensional model, *Journal of Marine Systems*, 16, 151–170, 1998.
- Morel, A.: Light and marine photosynthesis: a spectral model with geochemical and climatological implications, *Progress in Oceanography*, 26, 263–306, 1991.
- Morel, A. and Berthon, J.-F.: Surface pigments, algal biomass profiles, and potential production of the euphotic layer: Relationships reinvestigated in view of remote-sensing applications, *Limnology and Oceanography*, 34, 1545–1562, 1989.
- 590 Morel, A. and Maritorena, S.: Bio-optical properties of oceanic waters: A reappraisal, *Journal of Geophysical Research: Oceans*, 106, 7163–7180, 2001.
- Morel, A., Gentili, B., Chami, M., and Ras, J.: Bio-optical properties of high chlorophyll Case 1 waters and of yellow-substance-dominated Case 2 waters, *Deep Sea Research Part I: Oceanographic Research Papers*, 53, 1439–1459, 2006.
- 595 Morel, A., Huot, Y., Gentili, B., Werdell, P. J., Hooker, S. B., and Franz, B. A.: Examining the consistency of products derived from various ocean color sensors in open ocean (Case 1) waters in the perspective of a multi-sensor approach, *Remote Sensing of Environment*, 111, 69–88, 2007.
- Nightingale, P. D., Malin, G., Law, C. S., Watson, A. J., Liss, P. S., Liddicoat, M. I., Boutin, J., and Upstill-Goddard, R. C.: In situ evaluation of air-sea gas exchange parameterizations using novel conservative and volatile tracers, *Global Biogeochemical Cycles*, 14, 373–387, 600 2000.
- Ohde, T. and Siegel, H.: Correction of bottom influence in ocean colour satellite images of shallow water areas of the Baltic Sea, *International Journal of Remote Sensing*, 22, 297–313, 2001.
- Olita, A., Capet, A., Claret, M., Mahadevan, A., Poulain, P. M., Ribotti, A., Ruiz, S., Tintoré, J., Tovar-Sánchez, A., and Pascual, A.: Frontal dynamics boost primary production in the summer stratified Mediterranean Sea, *Ocean Dynamics*, 67, 767–782, 2017.
- 605 Parekh, P., Follows, M. J., Dutkiewicz, S., and Ito, T.: Physical and biological regulation of the soft tissue carbon pump, *Paleoceanography*, 21, 2006.
- Platt, T. and Sathyendranath, S.: Oceanic primary production: estimation by remote sensing at local and regional scales, *Science*, 241, 1613–1620, 1988.
- Queste, B. Y., Fernand, L., Jickells, T. D., Heywood, K. J., and Hind, A. J.: Drivers of summer oxygen depletion in the central North Sea, 610 *Biogeosciences*, 13, 1209–1222, 2016.
- Reed, D. C., Rassweiler, A., Carr, M. H., Cavanaugh, K. C., Malone, D. P., and Siegel, D. A.: Wave disturbance overwhelms top-down and bottom-up control of primary production in California kelp forests, *Ecology*, 92, 2108–2116, 2011.
- Robinson, C., Tilstone, G. H., Rees, A. P., Smyth, T. J., Fishwick, J. R., Tarran, G. A., Luz, B., Barkan, E., and David, E.: Comparison of in vitro and in situ plankton production determinations, *Aquatic Microbial Ecology*, 54, 13–34, 2009.
- 615 Roemmich, D., Alford, M., Claustre, H., Johnson, K., King, B., Moum, J., et al.: On the future of Argo: an enhanced global array of physical and biogeochemical sensing floats. *Front. Mar. Sci*, 6, 439, 2019.
- Salomons, W., Bayne, B. L., Duursma, E. K., and Förstner, U.: *Pollution of the North Sea: an assessment*, Springer Science & Business Media, 2012.

- Sathyendranath, S., Brewin, R. J., Brockmann, C., Brotas, V., Calton, B., Chuprin, A., Cipollini, P., Couto, A. B., Dingle, J., Doerffer, R.,
620 et al.: An ocean-colour time series for use in climate studies: the experience of the ocean-colour climate change initiative (OC-CCI),
Sensors, 19, 4285, 2019.
- Sathyendranath, S., Platt, T., Kovač, Ž., Dingle, J., Jackson, T., Brewin, R. J., Franks, P., Marañón, E., Kulk, G., and Bouman, H. A.:
Reconciling models of primary production and photoacclimation, Applied Optics, 59, C100–C114, 2020.
- Sathyendranath, S. et al.: Remote sensing of ocean colour in coastal, and other optically-complex, waters., Tech. rep., International Ocean
625 Colour Coordinating Group (IOCCG), 2000.
- Saulquin, B., Hamdi, A., Gohin, F., Populus, J., Mangin, A., and d’Andon, O. F.: Estimation of the diffuse attenuation coefficient KdPAR
using MERIS and application to seabed habitat mapping, Remote Sensing of Environment, 128, 224–233, 2013.
- Sauzède, R., Claustre, H., Jamet, C., Uitz, J., Ras, J., Mignot, A., and D’Ortenzio, F.: Retrieving the vertical distribution of chlorophyll a
concentration and phytoplankton community composition from in situ fluorescence profiles: A method based on a neural network with
630 potential for global-scale applications, Journal of Geophysical Research: Oceans, 120, 451–470, 2015.
- Sauzède, R., Claustre, H., Uitz, J., Jamet, C., Dall’Olmo, G., d’Ortenzio, F., Gentili, B., Poteau, A., and Schmechtig, C.: A neural network-
based method for merging ocean color and Argo data to extend surface bio-optical properties to depth: Retrieval of the particulate backscat-
tering coefficient, Journal of Geophysical Research: Oceans, 121, 2552–2571, 2016.
- Skákala, J., Ford, D., Bruggeman, J., Hull, T., Kaiser, J., King, R. R., Loveday, B., Palmer, M. R., Smyth, T., Williams, C. A., et al.: Towards
635 a multi-platform assimilative system for North Sea biogeochemistry, Journal of Geophysical Research: Oceans, 126, e2020JC016 649,
2021.
- Smith, R. N., Schwager, M., Smith, S. L., Jones, B. H., Rus, D., and Sukhatme, G. S.: Persistent ocean monitoring with underwater gliders:
Adapting sampling resolution, Journal of Field Robotics, 28, 714–741, 2011.
- Smyth, T., Fishwick, J., Gallienne, C., Stephens, J., and Bale, A.: Technology, design, and operation of an autonomous buoy system in the
640 western English Channel, Journal of Atmospheric and Oceanic Technology, 27, 2056–2064, 2010a.
- Smyth, T. J., Fishwick, J. R., Al-Moosawi, L., Cummings, D. G., Harris, C., Kitidis, V., Rees, A., Martinez-Vicente, V., and Woodward,
E. M.: A broad spatio-temporal view of the Western English Channel observatory, Journal of Plankton Research, 32, 585–601, 2010b.
- Swart, S., Thomalla, S. J., and Monteiro, P. M.: The seasonal cycle of mixed layer dynamics and phytoplankton biomass in the Sub-Antarctic
Zone: A high-resolution glider experiment, Journal of Marine Systems, 147, 103–115, 2015.
- 645 Taylor, J. R. and Ferrari, R.: Ocean fronts trigger high latitude phytoplankton blooms, Geophysical Research Letters, 38, 2011.
- Testor, P., De Young, B., Rudnick, D. L., Glenn, S., Hayes, D., Lee, C. M., Pattiaratchi, C., Hill, K., Heslop, E., Turpin, V., et al.: OceanGlid-
ers: a component of the integrated GOOS, Frontiers in Marine Science, p. 422, 2019.
- Thomalla, S. J., Racault, M.-F., Swart, S., and Monteiro, P. M.: High-resolution view of the spring bloom initiation and net community
production in the Subantarctic Southern Ocean using glider data, ICES Journal of Marine Science, 72, 1999–2020, 2015.
- 650 Thomalla, S. J., Moutier, W., Ryan-Keogh, T. J., Gregor, L., and Schütt, J.: An optimized method for correcting fluorescence quenching using
optical backscattering on autonomous platforms, Limnology and Oceanography: Methods, 16, 132–144, 2018.
- van Beusekom, J. and Diel-Christiansen, S.: A synthesis of phyto and zooplankton dynamics in the North Sea environment, WWF reports,
1994.
- Varela, R. A., Cruzado, A., and Gabaldón, J. E.: Modelling primary production in the North Sea using the European regional seas ecosystem
655 model, Netherlands Journal of Sea Research, 33, 337–361, 1995.

- Wanninkhof, R.: Relationship between wind speed and gas exchange over the ocean, *Journal of Geophysical Research: Oceans*, 97, 7373–7382, 1992.
- Wojtasiewicz, B., Walsh, I. D., Antoine, D., Slawinski, D., and Hardman-Mountford, N. J.: Inferring and removing a spurious response in the optical backscattering signal from an autonomous profiling float, *Journal of Atmospheric and Oceanic Technology*, 35, 2137–2146, 2018.
- 660 Xing, X., Claustre, H., Blain, S., d’Ortenzio, F., Antoine, D., Ras, J., and Guinet, C.: Quenching correction for in vivo chlorophyll fluorescence acquired by autonomous platforms: A case study with instrumented elephant seals in the Kerguelen region (Southern Ocean), *Limnology and Oceanography: Methods*, 10, 483–495, 2012.
- Zhao, C., Daewel, U., and Schrum, C.: Tidal impacts on primary production in the North Sea, *Earth System Dynamics*, 10, 287–317, 2019.

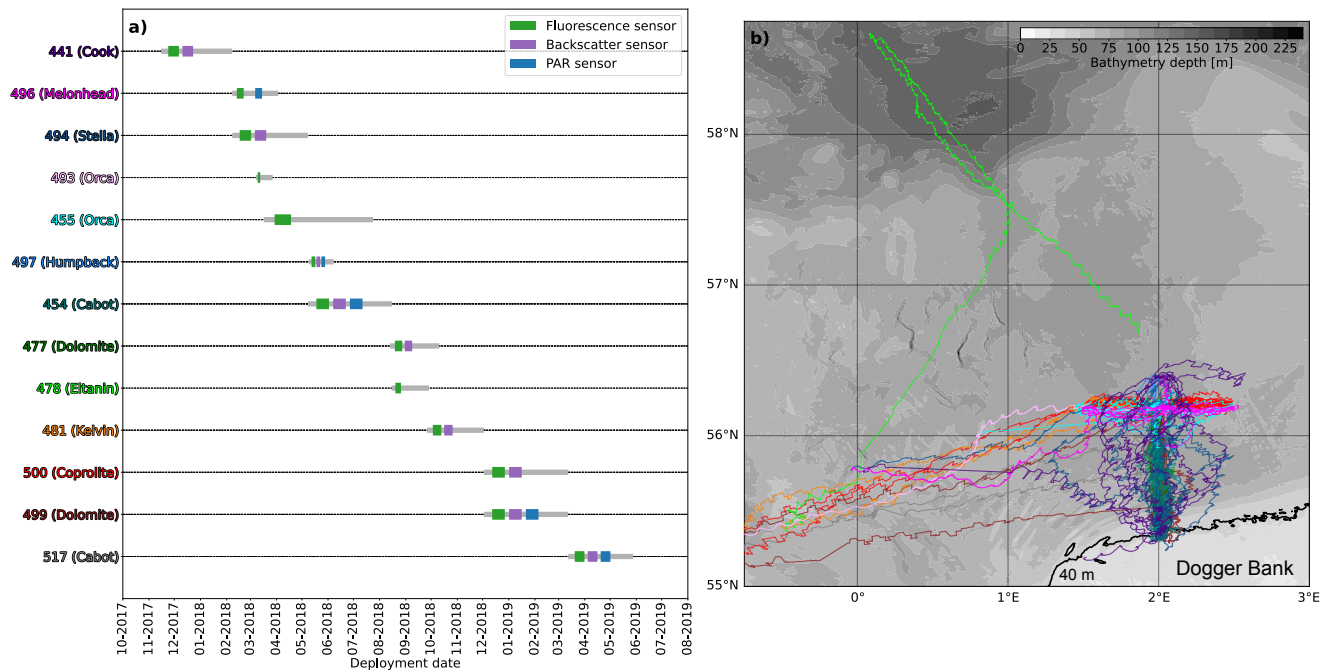


Figure 1. a) Overview of the AlterEco glider deployment schedule and sensor payloads relevant to primary production calculations. b) Trajectories of glider deployments overlaid on the General Bathymetric Chart of the Oceans (GEBCO) 2020-2021 15'' bathymetry for the North Sea. Track colours match the respectively coloured glider name from panel (a) (and with [Figure ?? figure 9](#)), with warmer track colours corresponding to later deployments. The 40 m contour, shown in black, nominally represents the outer edges of Dogger Bank.

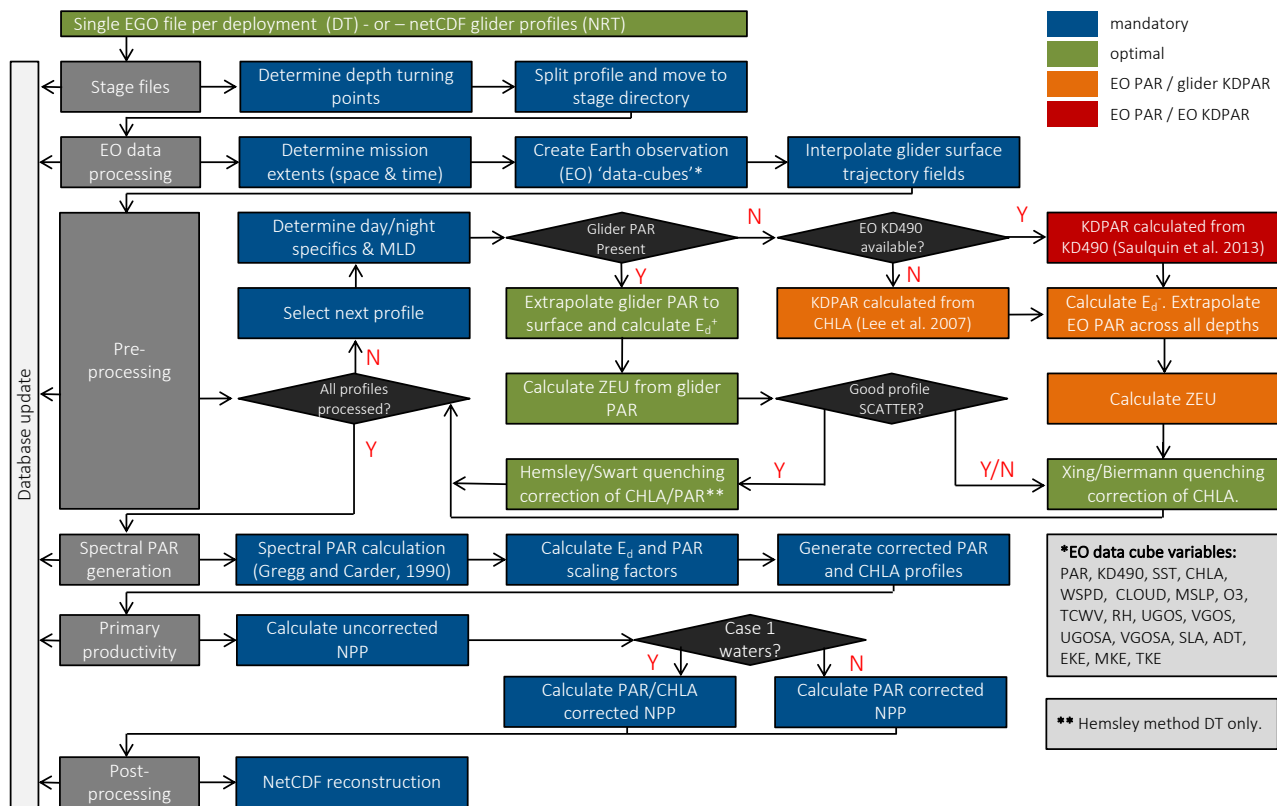


Figure 2. Schematic overview of the glider-based primary production processing chain. Blue boxes indicate mandatory steps; Green, orange and red boxes indicate processing options in order of decreasing preference. The light grey inset box describes the Earth observation variables that are interpolated onto a glider's path.

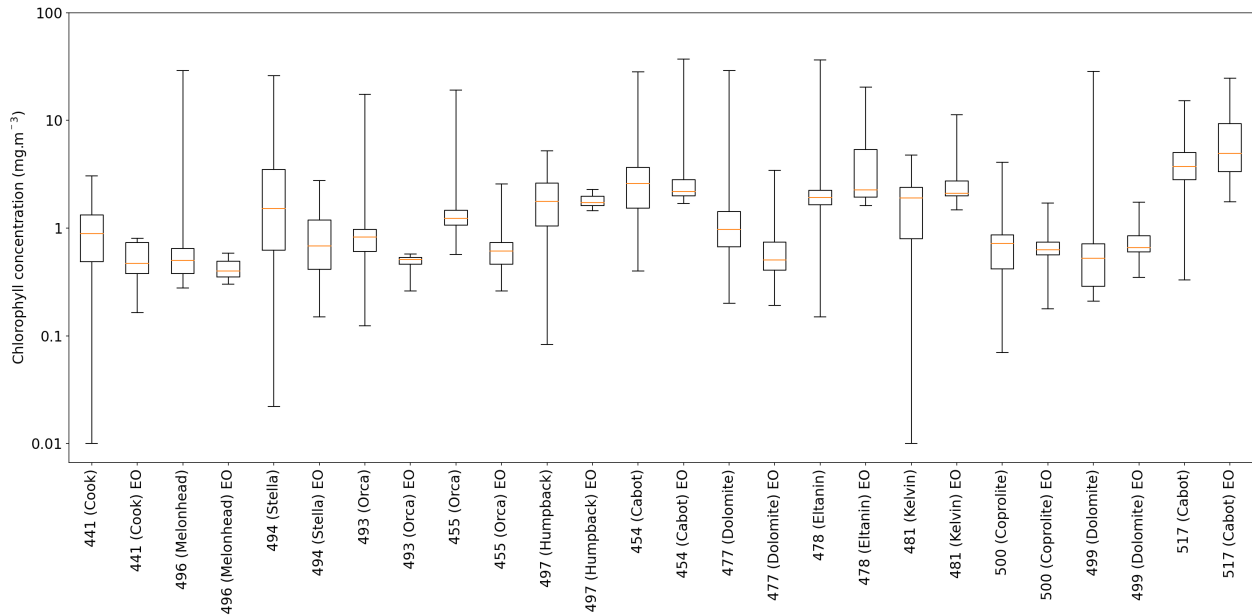


Figure 3. Statistical comparison of the surface chlorophyll values measured by each glider with its SEO trajectory counterpart. From bottom to top, the box and whisker plot show the values shown are the minimum, lower quartile range (25%), median, upper quartile range (75%) and maximum. Only the glider measurements with an SEO counterpart are considered.

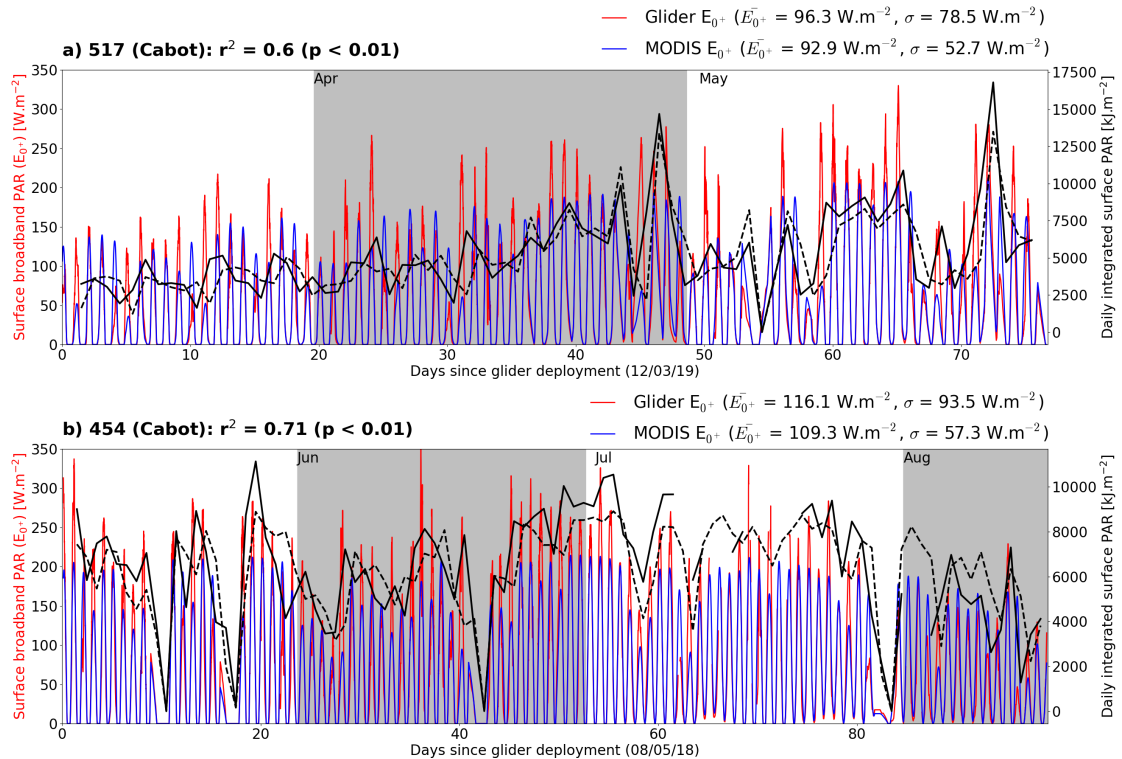


Figure 4. Comparison of glider and MODIS based surface broadband PAR (E_{0+}) values. Red and blue traces show the 10-profile smoothed PAR for the glider and interpolated MODIS products, respectively. These are recorded against the left hand axis. All statistics (r^2 , μ , σ) are based on the valid, unsmoothed time-series data, for day-time profiles only. The solid and dashed black traces, measured against the right hand axis, show the daily integrated PAR values for the glider and MODIS products, respectively, and are derived from the corresponding red and blue traces.

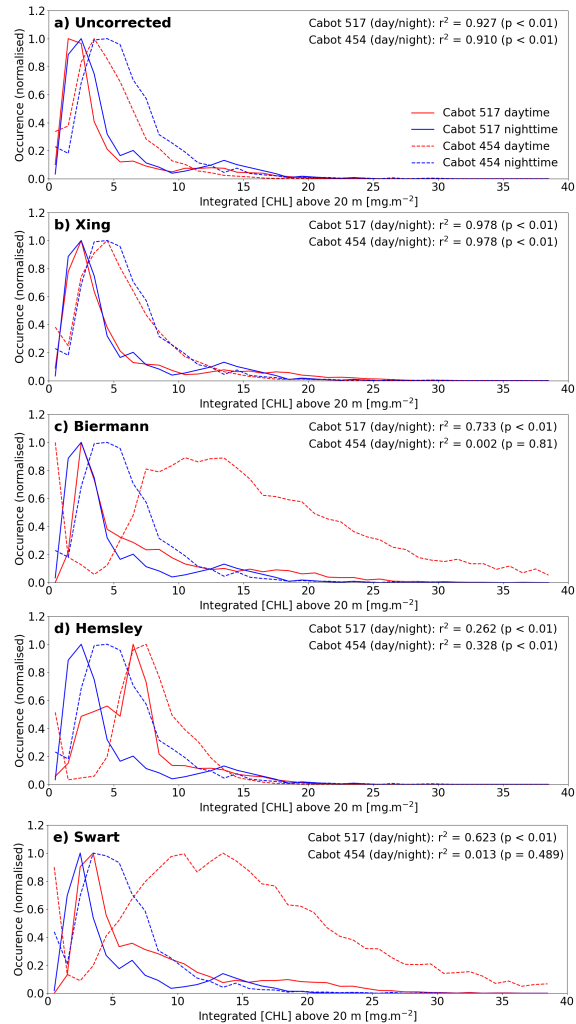


Figure 5. The effects of the implementation of different quenching mechanisms on the distribution of the integrated [Chl-a] in the top 20 m for Cabot deployments 454 (dashed lines) and 517 (solid lines). Panel a) shows the distribution of day-time (red) and night time (blue) [Chl-a] in the uncorrected case. Panels b), c) and d) and e) show the effects of implementing the mixed layer depth based correction of Xing et al. (2012), euphotic depth based correction of Biermann et al. (2015), and scattering the backscatter based correction corrections of Hemsley et al. (2015) and Swart et al. (2015)

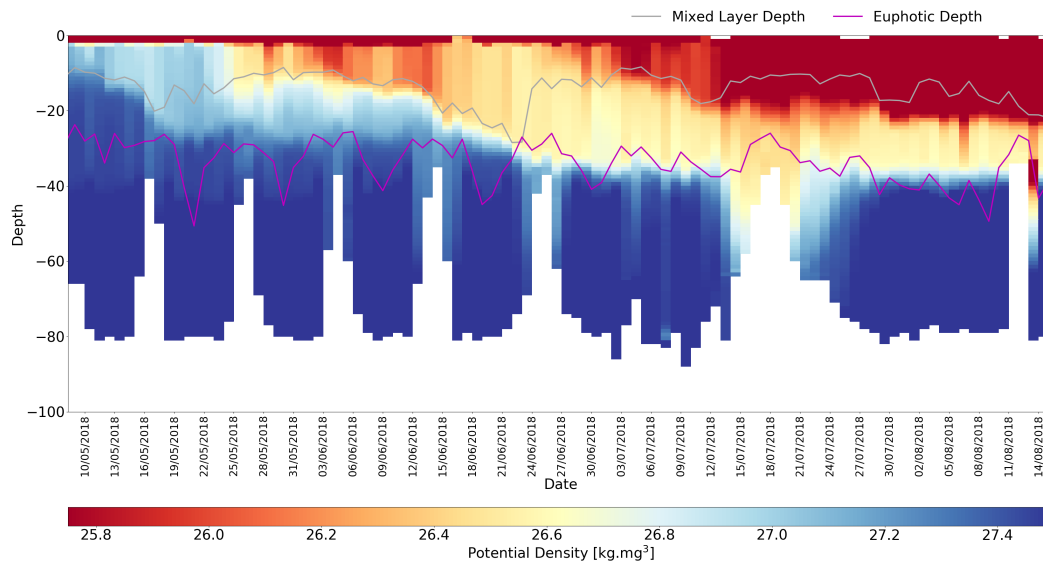


Figure 6. Potential density distribution for time series for 454 (Cabot). Mixed layer depth and euphotic depths are shown by the respective grey and purple traces, which have been smoothed using a 10 profile window. Gaps in the euphotic depth time series correspond to night-time profiles.

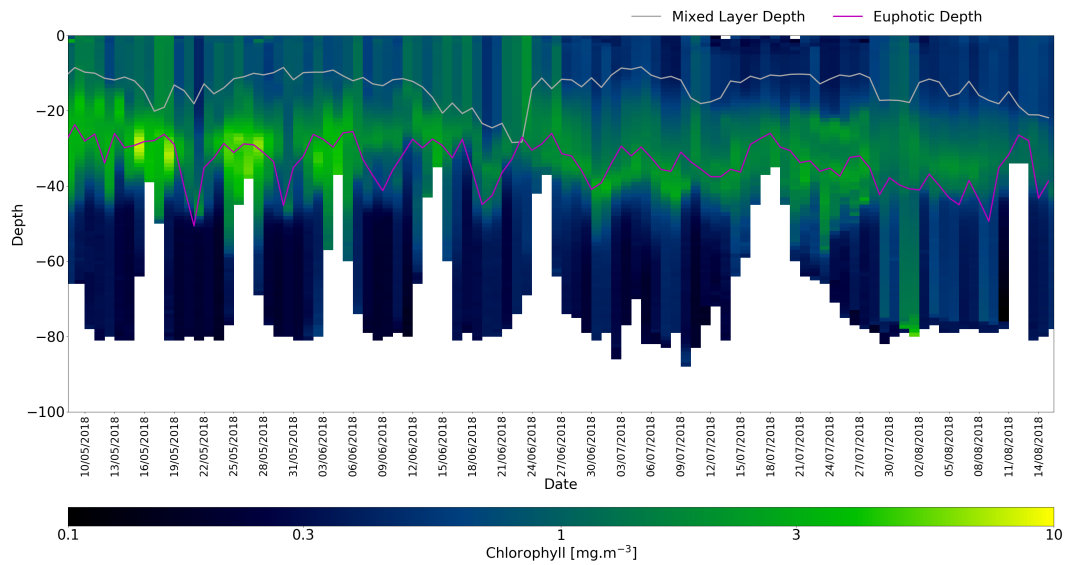


Figure 7. Quenching corrected [Chl-a] time series for 454 (Cabot). The Xing et al. (2012) quenching corrected is applied. Mixed layer depth and euphotic depths are as in figure ??6).

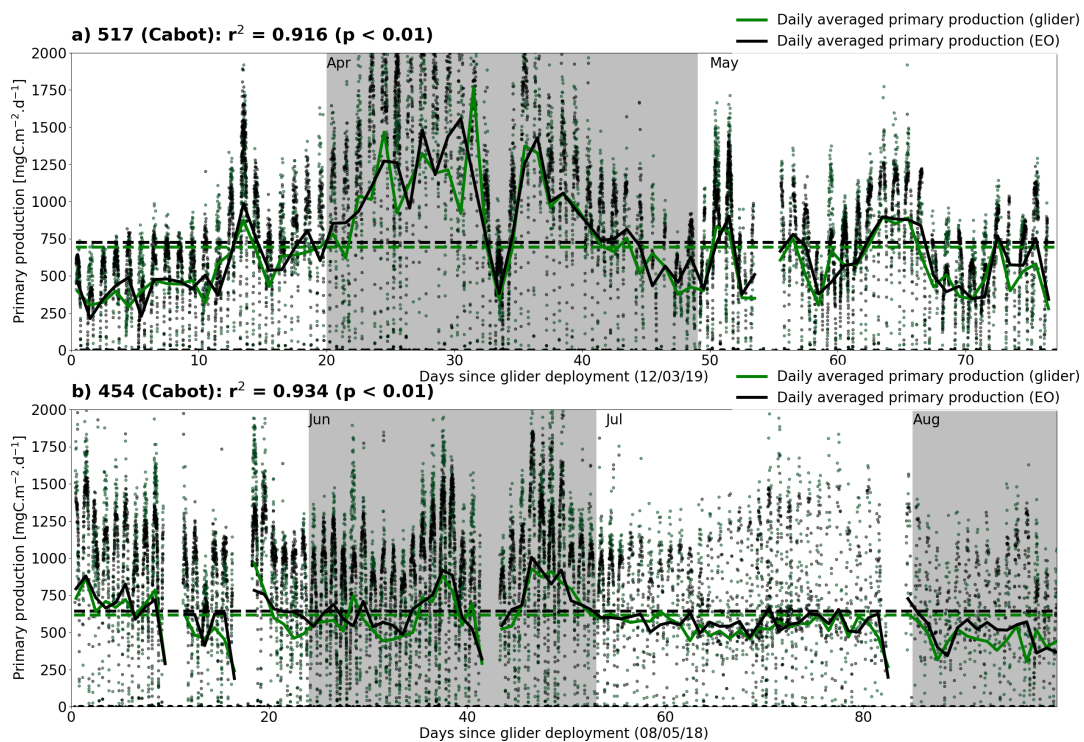
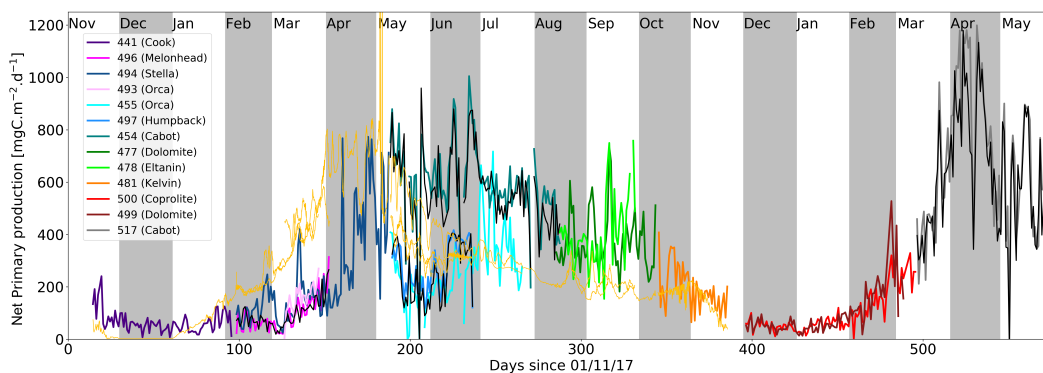


Figure 8. Comparison of net primary production estimates from the *in-situ* based PAR method (green points and traces) and SEO-based PAR method (black points and traces) for glider Cabot for missions a) 517 and b) 454. Points represent the instantaneous measurements taken from individual profiles, with solid traces showing the daily integrated values. Total mean daily values for each mission and method are given by the respective dashed lines. The r^2 statistic is calculated between the individual profile values for the two methods.

Daily integrated net primary production estimates from all gliders deployed in the AlterEco programme (see table 1). Coloured traces represent each glider mission (matching those used in figure 1), and show the net primary production estimates derived from the SEO-based PAR method. Where *in situ* PAR sensors were available, a corresponding black trace for that glider mission is also



shown.

Figure 9. Daily integrated net primary production estimates from all gliders deployed in the AlterEco programme (see table 1). Coloured traces represent each glider mission (matching those used in figure 1), and show the net primary production estimates derived from the SEO-based PAR method. Where *in situ* PAR sensors were available, a corresponding black trace for that glider mission is also shown. The thin orange trace shows the net primary production extracted from v4.2 of the OC-CCI NPP product for each glider, where available.

Table 1. An overview of mission nomenclature. All glider data used in the calculation of primary production is available at https://www.bodc.ac.uk/data/bodc_database/gliders/ and ~~is~~ ~~are~~ published ~~under~~ ~~at~~ the following ~~doi~~ ~~s~~ ~~urls~~: <https://doi.org/10.5285/b57d215e-065f-7f81-e053-6c86abc01a82> and <https://doi.org/10.5285/86429662-97b8-74fa-e053-6c86abc0a97c>

Campaign	Platform	Deployment	Glider serial	Processed here	Source data link
AlterEco1	Fin	439	SG537	No, incompatible sensor-load sensors	Fin_439_R.nc
	Stella	440	unit_436	No, incompatible sensor-load early recovery	N/A
	Cook	441	unit_194	Yes	Cook_441_R.nc
AlterEco2	Orca	493	SG510	Yes	Orca_493_R.nc
	Stella	494	unit_436	Yes	Stella_494_R.nc
	OMG-1	495	unit_352	No, incompatible sensor-load sensors	OMG-1_495_R.nc
	Melonhead	496	sg620	Yes	Melonhead_496_R.nc
AlterEco3	Cabot	454	unit_345	Yes	Cabot_454_R.nc
	Orca	455	SG510	Yes	Orca_455_R.nc
	Humpback	497	SG579	Yes	Humpback_497_R.nc
	Lyra	486	999	No, incompatible sensor-load sensors	N/A
AlterEco4	Dolomite	477	unit_305	Yes	Dolomite_477_R.nc
	Eltanin	478	SG550	Yes	Eltanin_478_R.nc
	Scapa	479	SG602	No, incompatible sensor-load sensors	Scapa_479_R.nc
	Lyra	480	999	No, incompatible sensor-load sensors	N/A
AlterEco5	Kelvin	481	unit_444	Yes	Kelvin_481_R.nc
AlterEco6	Dolomite	499	unit_305	Yes	Dolomite_499_R.nc
	Coprolite	500	unit_331	Yes	Coprolite_500_R.nc
AlterEco7	Ammonite	516	unit_304	No, incompatible sensor-load sensors	Ammonite_516_R.nc
	Cabot	517	unit_345	Yes	Cabot_517_R.nc
	Scapa	518	SG602	No, incompatible sensor-load sensors	Scapa_518_R.nc

Table 2. Glider dive specifics per mission. The maximum profile distance is calculated from the maximum dive depth and mean dive angle and gives the maximum horizontal extent of a single dive (both down and up profiles).

<u>Platform</u>	<u>Deployment</u>	<u>Mean/Max dive depth (m)</u>	<u>Mean dive angle</u>	<u>Maximum profile distance (m)</u>
<u>Cook</u>	<u>441</u>	<u>39.91 / 91.85</u>	<u>24.60</u>	<u>401.29</u>
<u>Orca</u>	<u>493</u>	<u>42.05 / 95.54</u>	<u>16.01</u>	<u>666.10</u>
<u>Stella</u>	<u>494</u>	<u>35.13 / 94.24</u>	<u>24.11</u>	<u>421.25</u>
<u>Melonhead</u>	<u>496</u>	<u>42.90 / 92.53</u>	<u>20.19</u>	<u>503.29</u>
<u>Cabot</u>	<u>454</u>	<u>33.34 / 82.29</u>	<u>24.69</u>	<u>358.04</u>
<u>Orca</u>	<u>455</u>	<u>43.89 / 96.89</u>	<u>15.04</u>	<u>721.13</u>
<u>Humpback</u>	<u>497</u>	<u>44.51 / 87.31</u>	<u>12.58</u>	<u>782.22</u>
<u>Dolomite</u>	<u>477</u>	<u>34.70 / 83.38</u>	<u>24.36</u>	<u>368.22</u>
<u>Eltanin</u>	<u>478</u>	<u>44.10 / 97.74</u>	<u>15.37</u>	<u>711.35</u>
<u>Kelvin</u>	<u>481</u>	<u>37.31 / 87.22</u>	<u>27.09</u>	<u>340.99</u>
<u>Dolomite</u>	<u>499</u>	<u>36.52 / 87.35</u>	<u>24.30</u>	<u>386.83</u>
<u>Coprolite</u>	<u>500</u>	<u>40.90 / 89.61</u>	<u>24.44</u>	<u>394.29</u>
<u>Cabot</u>	<u>517</u>	<u>32.65 / 82.90</u>	<u>24.17</u>	<u>369.42</u>

Table 3. List of SEO and reanalysis variables used to support glider missions. Bold type variables are derived by the primary production processor.

Description	Provider	Source	Variables
Sea surface topography	CMEMS	SEALEVEL_GLO_PHY_L4_NRT & REP	sea-level anomaly absolute dynamic topography absolute geostrophic velocities geostrophic velocities anomalies eddy kinetic energy total kinetic energy mean kinetic energy
Atmospheric variables	ECMWF	ERA-I	10 m wind speed (u/v) total cloud cover mean sea level pressure [O ₃] [water vapour] 2 m temperature 2 m dew point wind speed relative humidity
Optical variables	NASA	MODIS L3m Daily products	PAR K _{d490} instantaneous PAR
Ocean tracers	CMEMS	GLOBAL_ANALYSIS_FORECAST_PHY	sea surface temperature sea surface salinity mixed layer depth
Biogeochemistry	CMEMS	OCEANCOLOUR_GLO_CHL_L3_NRT & REP	[CHLA] euphotic depth

Table 4. Variables present in the EGO format netCDF data files. All variables have a single 'time' dimension.

Variable name	Quantity	Units
TIME	time	seconds since 1970-01-01
PROFILE_NUMBER	glider profile number	none
LONGITUDE	longitude	degrees east
LATITUDE	latitude	degrees north
PRESSURE	pressure	decibar
DEPTH	glider depth	m
CHLA	quenching corrected [CHL-a]	mg m ⁻³
MIXED_LAYER_DEPTH	mixed layer depth	m
EUPHOTIC_DEPTH	Euphotic depth (ZEU)	m
EUPHOTIC_DEPTH_FLAG	Euphotic depth method flag	none
DOWNWELLING_PAR	photosynthetically active radiation (PAR)	W m ⁻²
DOWNWELLING_PAR_FLAG	PAR method flag	none
DOWNWELLING_PAR_EO	PAR from satellite Earth observation (SEO)	W m ⁻²
DOWNWELLING_PAR_EO_FLAG	SEO PAR method flag	none
PRIMARY_PRODUCTION	Primary production (PP) from in situ <i>in situ</i> PAR	carbon flux of mg m ⁻³ d ⁻¹
PRIMARY_PRODUCTION_EO	PP from SEO PAR	carbon flux of mg m ⁻³ d ⁻¹
DEPTH_INTEGRATED_PRIMARY_PRODUCTION	PP integrated to ZEU	carbon flux of mg m ⁻² d ⁻¹
DEPTH....._PRODUCTION_EO	SEO PP integrated to ZEU	carbon flux of mg m ⁻² d ⁻¹

Note; DOWNWELLING_PAR_FLAG and DOWNWELLING_PAR_EO_FLAG are equivalent, but are included twice as they are relevant to both of their associated variables.

Table 5. Monthly statistics for SEO-PAR based depth integrated primary production estimates across all glider missions. Values for *in-situ* PAR based depth integrated primary production estimates are given in brackets, where available. All measurements are given in carbon flux, measured in $\text{g m}^{-2} \text{d}^{-1}$, unless otherwise specified. The final column gives the mean primary production extracted from v4.2 of the monthly OC-CCI climatology from 01/01/1998 to 31/12/2018 over a box spanning the core of the AlterEco sampling region (1.5°E to 2.5°E , 55.25°N to 56.25°N).

Month	NPP Mean	NPP Std. deviation	N profiles	OC-CCI NPP Mean*	OC-CCI NPP std. dev.*
January	53	21	8190	64	69
February	138 (70)	139 (23)	9925 (2381)	166	31
March	192 (184)	125 (131)	10868 (5105)	358	79
April	470 (607)	269 (251)	7393 (3336)	617	112
May	391 (416)	157 (158)	9382 (7132)	594	131
June	406 (476)	110 (142)	7951 (5916)	340	73
July	364 (397)	127 (138)	1634 (1498)	303	49
August	334 (344)	83 (74)	3928 (628)	278	58
September	317	91	4165	234	51
October	192	73	2923	177	31
November	134	50	2554	109	55
December	49	16	5276	4	13
Annual	269	199	74189	270	63
Annual ($\text{mg m}^{-2} \text{d}^{-1}$)	269	199	74189	270	63
Annual ($\text{g m}^{-2} \text{a}^{-1}$)	98	73	74189	99	23

*Data provided by Plymouth Marine Laboratory, based on Kulk et al. (2020)